Rotation-dependent epitaxial relations between graphene and the Si-terminated SiC substrate

V. Sorkin* and Y. W. Zhang
Institute of High Performance Computing, Singapore 138632, Singapore

(Received 18 February 2010; revised manuscript received 23 June 2010; published 23 August 2010)

We study the rotation-dependent epitaxial relations between graphene nanoflake and the Si-terminated 4H-SiC(0001) substrate. Depending on the rotation angle between the nanoflake and substrate surface, we find that Si-C bonds formed between the C atoms in the nanoflake and Si atoms on the SiC surface exhibit complicated two-dimensional patterns. Among the various patterns formed, we reveal a finite-size epitaxial domain with a perfectly regular triangular lattice. We further identify the lattice constant of 12.3 Å and the maximal size of the perfect lattice domain is about 70 Å. It is found that the maximal lattice domain size is set by the lattice mismatch between the common hexagonal lattices of the graphene nanoflake and its underlying substrate.

DOI: 10.1103/PhysRevB.82.085434 PACS number(s): 62.23.Kn, 81.07.Ta, 68.37.Ef, 62.23.Eg

I. INTRODUCTION

Graphene[1,2] is a one-atom-thick allotrope of carbon which has received much attention recently.[3,4] Thanks to its remarkable electronic, magnetic, and thermomechanical properties, graphene is the material of substantial interest for many potential applications in nanoscale mechanics, electronics, and spintronics.[5–8]

Recently carbon nanoflakes, graphene-derived structures, have attracted a considerable research interest. The nanoflakes provide a new route to carbon-based nanoelectronics. It was shown that nanoflakes have fascinating electronic[9–14] and magnetic properties determined by their shape and edge structures.[15,16] Confined electron spins of graphene nanoflakes were suggested by Trauzettel *et al.*[17] to use as carriers of quantum information (qubits). The magnetic properties of graphene nanoflakes open numerous possibilities for applications in carbon-based spintronics. Ponomarenko *et al.*[18] designed graphene nanotransistor based on a graphene quantum dot,[19–22] which is a graphene nanoflake made of only a few benzene rings. Graphene quantum dots, in which the electronic properties can be tuned from semimetallic to semiconducting with a substantial and controllable band gap, provide new possibilities to control transport of charge carriers in nanodevices.[23,24]

In electronic applications, nanoflakes may also serve as templates for nanodevices. In this case, graphene nanoflakes have to be accommodated on a substrate. However, in the presence of a substrate, the morphology and properties of graphene nanoflake may be changed, much like morphology and properties of graphene being affected by its underlying substrate. Lately, the epitaxial relations between graphene and its underlying substrate have been a subject of intense research.[25–28] It was found that initial graphene morphology could be modified by covalent-bond formation at the graphene-substrate interface. In our preceding work,[29] we explored the morphology of a graphene nanoribbon supported by an Si-terminated SiC(0001) substrate. It was displayed that the planar shape of the graphene was substantially distorted by the underlying substrate. Appreciable ripples were created in the graphene nanoribbon due to the combined effect of the van der Waals interaction and covalent-bond formation between the graphene nanoribbon and the substrate.

The epitaxial relations between the finite-size graphene nanoflake and the substrate surface can be even more complicated due to the presence of the translational and rotational degrees of freedom of the nanoflake. These relations have not been studied systematically. Being aware of the substantial interest to the effect of substrate on the morphology of nanoflakes, we investigated epitaxial relations between graphene nanoflake and the Si-terminated 4H-SiC(0001) substrate. Our attention is given to patterns of Si-C covalent bonds formed at the nanoflake-substrate interface. We found a variety of complex bond patterns formed as a graphene nanoflake is rotated on the substrate. Most interesting, an epitaxial domain with perfectly triangular lattice was identified and investigated in details.

In the following, we first present our computational model, followed by the presentation of the results discussion. Finally, we present the conclusions.

II. COMPUTATIONAL MODEL

In our simulations, a graphene nanoflake disk of a given radius is placed on the top of the Si-terminated substrate (see Figs. 1 and 2). The 4H-SiC(0001) substrate is represented by six carbon-silicon bilayers (see Fig. 1). Periodic boundary conditions are applied along the X and Y directions (Fig. 10). Two SiC bilayers are fixed at the sample bottom to mimic a semi-infinite substrate along the Z direction. The X axis of the Cartesian coordinate system associated with the SiC substrate is oriented along the $[\bar{1}2\bar{1}0]$ direction and the Y axis is along the $[\bar{1}010]$ one, where Miller-Bravais indices[30] are used for directions. The graphene nanoflake disk is cut from a graphene sheet. Initially, its reference frame coincides with the coordinate system associated with the substrate, as shown

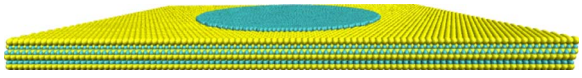

FIG. 1. (Color online) Sample geometry (side view): a graphene nanoflake on the top of the Si-terminated 4H-SiC(0001) substrate. Radius of the graphene nanoflake is 72 Å. The carbon atoms of the graphene nanoflake are marked by cyan color and the silicon atoms of the underlying substrate are marked by yellow color.

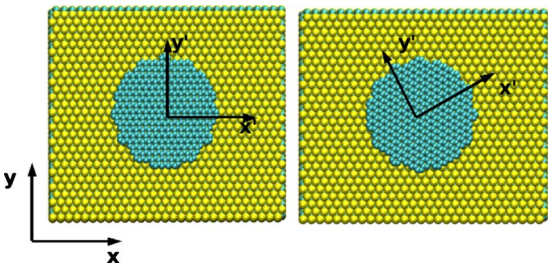

FIG. 2. (Color online) Graphene nanoflake disk on the Si-terminated SiC(0001) substrate (top view). (a) In the initial configuration the rotation angle is set to $\theta=0°$ (b) A configuration in which the graphene nanoflake is rotated by $\theta=30°$. The (X,Y) reference frame is associated with the substrate and the (X',Y') frame is associated with the nanoflake disk. The radius of the graphene nanoflake disk is 20 Å. The carbon atoms of the graphene nanoflake are marked by cyan color and the silicon atoms of the underlying substrate are marked by yellow color.

in Fig. 2(a). Two unit-cell basis vectors, a_1 and a_2, of graphene are given in this frame by

$$a_1 = \left(\frac{\sqrt{3}}{2}, \frac{1}{2}\right)a, \tag{1}$$

$$a_2 = \left(\frac{\sqrt{3}}{2}, -\frac{1}{2}\right)a, \tag{2}$$

where $a=2.46$ Å is the lattice constant of graphite, related to the carbon-carbon bond length, $a_{C\text{-}C}$, by $a=\sqrt{3}a_{C\text{-}C}$. This choice sets the initial position and the zero rotation angle for the nanoflake disk. In what follows the graphene nanoflake disk is rotated on the SiC substrate in the counterclockwise direction as shown in Fig. 2(b).

The radius of the graphene nanoflake disk, R, is varied from $R=24$ Å to $R=184$ Å. The lateral substrate size is varied to adapt to variation in the nanoflake radius. The number of atoms in the nanoflakes is varied between $N=4283$ up to $N=340\,321$, accordingly. The distance between the graphene nanoflake and substrate is set initially to $Z=2.3$ Å. This distance is chosen to provide the fastest convergence to the total-energy minimum using conjugate-gradient minimization. We verified that the results of our calculations are independent of this particular choice.

A semiempirical many-body potential introduced by Tersoff[31] is used to describe the C-C, C-Si, and Si-Si interatomic interactions. This potential has been recently successfully employed to study carbon nanotubes,[32,33] fullerenes,[34] silicon nanotubes,[35] and silicon carbide.[36]

Conjugate gradient method is applied to minimize the total energy of the sample at zero temperature. Subsequently we investigate the morphology of a graphene nanoflake supported by the Si-terminated SiC(0001) substrate. The conjugate gradient method is implemented as a part of the large-scale atomic/molecular massively parallel simulator (LAMMPS) code,[37] which is used in our simulations.

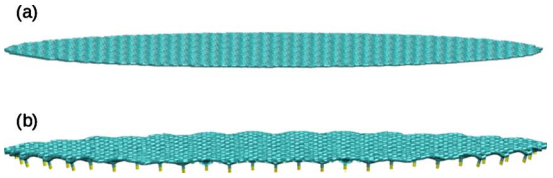

FIG. 3. (Color online) Ripples in a graphene nanoflake accommodated on the Si-terminated 4H-SiC(0001) substrate. (a) Initial planar shape of the graphene nanoflake with radius 72 Å. (b) Final shape of the graphene nanoflake after conjugate-gradient minimization of the total energy of the system. Covalent bonds are formed at the interface between the graphene nanoflake and its underlying substrate.

III. RESULTS AND DISCUSSION

We place a graphene nanoflake on the Si-terminated 4H-SiC(0001) surface and minimize the total energy of the system at zero temperature. The initial planar shape of graphene nanoflake [see Fig. 3(a)] is apparently altered by the underlying silicon-carbide substrate. Ripples emerge in the graphene nanoflake [see Fig. 3(b)] as the minimum-energy configuration is attained. These ripples appear mainly due to the combined effect of the van der Waals repulsion and bond formation at the graphene nanoflake-substrate interface. The average bond length of the Si-C bonds formed between the graphene nanoflake and the substrate is about $d_{Si\text{-}C}=1.88$ Å, which is very close to the covalent-bond length in silicon carbide $d_{Si\text{-}C}=1.89$ Å.[38] We note that a Si-C covalent bond is formed only if the initial distance between a pair of atoms making the bond is sufficiently small, i.e., the electronic orbitals of the bond forming atoms overlap. A Si-C bond is identified if the distance between the two atoms is less than a critical limit. This upper limit for the Si-C bond length should take into account the maximum allowable mechanical stretch of a Si-C bond. When a Si-C bond is stretched beyond the limit, it becomes unstable and breaks apart. Our calculation shows that this upper limit of the bond length is 1.95 Å.

The ripples emerging in graphene nanoflakes are very similar to the ripples previously found in nanoribbons supported by the Si-terminated SiC(0001) substrate. The properties of ripples formed in nanoribbons supported by the Si-terminated SiC(0001) substrate were thoroughly investigated in our earlier work.[29] The ripples emerging here in the graphene nanoflakes are similar to those found in the nanoribbons.

Although the ripples appearing in the graphene nanoflake resemble those in free-standing graphene nanoribbons, which have been extensively investigated,[39–43] the physical origins for the formation of these two types of ripples are different. In a free-standing graphene nanoflake, the change in the bonding environment along the edges leads to edge stress, which is compressive along the armchair and zigzag edges.[39] The relaxation of the compressive edge stress results in ripple formation near the edges in a free-standing graphene. For the substrate-supported graphene, the compressive edge stress plays only a minor role. Our previous simulations[29] showed that the main cause of the ripple formation of a

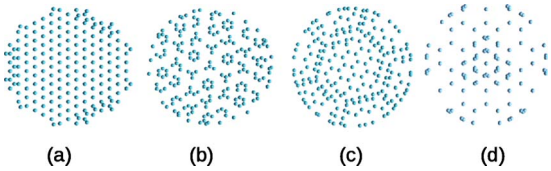

FIG. 4. (Color online) Geometrical patterns of covalent Si-C bonds formed at the graphene nanoflake-substrate interface as a function of the rotation angle, θ: (a) $\theta=0°$, (b) $\theta=5°$, (c) $\theta=10°$, and (d) $\theta=30°$. Radius of the graphene nanoflake is 84 Å.

graphene nanoflake on the Si-terminated SiC(0001) substrate is the combined effect of the covalent-bond formation and the van der Waals interactions between the graphene nanoflake and the underlying surface. Although the amplitudes of the ripples in the two cases are comparable, the intrinsic wavelengths of these two are quite different: the wavelength in a free-standing graphene is about 60–80 Å,[39] while it is only about 20–30 Å in a graphene nanoflake supported by the substrate.[29]

The established Si-C covalent bonds form various two-dimensional patterns at the interface between the graphene nanoflake and the underlying substrate. To visualize the geometrical structure of a typical pattern, we plot in-plane distribution of the Si-C covalent bonds at the interface. When nanoflake is rotated around a vertical axis passing through its origin, the bond pattern changes. The observed geometrical patterns are a function of the rotation angle (see Fig. 4).

To investigate stability of these patterns, we calculate for each pattern the energy per bond, E_b, as a function of a rotation angle according to

$$E_b = \frac{E_{tot} - E_{sub} - E_{fl}}{N_b}, \tag{3}$$

where E_{tot} is the total energy of the sample, E_{sub} is the substrate energy, E_{fl} is energy of the graphene nanoflake, and N_b is the number of bonds. The calculated energy per bond for the graphene nanoflake with the radius $R=84$ Å is shown in Fig. 5. As can be inferred from the Fig. 5 these patterns should be stable at low temperatures as the energy per bond is much higher than the average thermal energy at the room temperature, which is about 26 meV. At much higher temperatures, however, the pattern at $\theta=0°$ rotation angle should

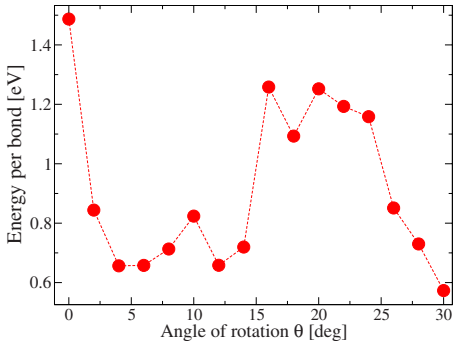

FIG. 5. (Color online) Energy per Si-C bond as a function of a rotation angle θ. The dashed line is to guide the eyes.

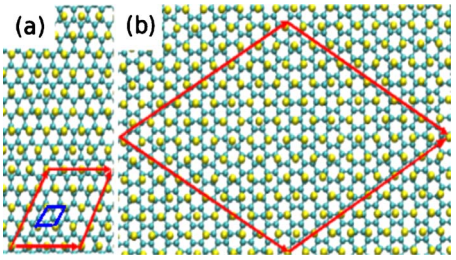

FIG. 6. (Color online) (a) The enlarged unit cell of the $p(4\times4)$ pattern formed by the overlapping silicon and carbon atoms (large parallelogram) and the original unit cell of the top substrate layer (small parallelogram). (b) The unit cell of the $6\sqrt{3}\times6\sqrt{3}R30°$ pattern formed by the overlapping silicon and carbon atoms. The carbon atoms of the graphene nanoflake are marked by cyan color and the silicon atoms of the underlying substrate are marked by yellow color.

be the most stable one, since its energy per bond is the highest. On the contrary, the pattern at $\theta=30°$ should be the least stable one as its energy per bond is the lowest.

For the rotation angle $\theta=0°$, a triangular lattice with the $p(4\times4)$ unit cell is identified. The unit cell of the identified pattern is obtained by magnifying four times the original (primitive) unit cell as shown in Fig. 6(a). The corresponding triangular lattice is shown in Fig. 7(a).

For the rotation angle $\theta=30°$, a lattice pattern with $6\sqrt{3}\times6\sqrt{3}R30°$ structure, as shown in Fig. 6(b), is identified. The $6\sqrt{3}\times6\sqrt{3}R30°$ notation specifies how the new unit cell of the identified pattern can be obtained from the original unit cell of the lattice formed by silicon atoms of the top substrate layer. The new unit cell is obtained by magnifying $6\sqrt{3}$ times the lattice vectors of the original unit cell with the subsequent rotation of the magnified unit cell by 30°. The observed lattice with the pattern $6\sqrt{3}\times6\sqrt{3}R30°$ is shown Fig. 8(a).

We can understand why Si-C bonds form the patterns with $p(4\times4)$ and $6\sqrt{3}\times6\sqrt{3}R30°$ structure by taking into account the sufficient conditions for Si-C bond formation and the lattice geometry of the graphene nanoflake and the substrate. Since a Si-C bond is formed between a pair of closely spaced atoms—we can predict possible bond patterns by identifying all Si-C pairs of the overlapping atoms at the interface in the

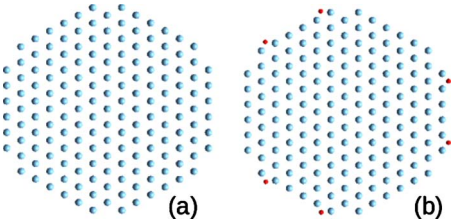

FIG. 7. (Color online) (a) Initial configuration: geometrical pattern $p(4\times4)$ formed by the overlapping silicon and carbon atoms. (b) Final configuration: geometrical pattern of Si-C bonds established at the graphene nanoflake-substrate interface. The bonds formed by the initially overlapping atoms are marked by blue cyan and the bonds formed by the atoms which do not overlap in the initial configuration are marked by red color. The rotation angle is $\theta=0°$ and the radius of the graphene nanoflake is $R=84$ Å.

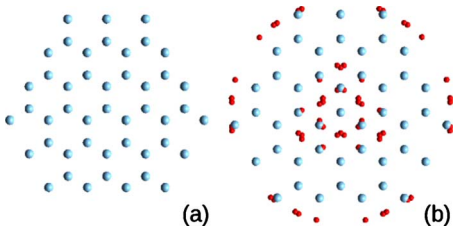

FIG. 8. (Color online) (a) Initial configuration: geometrical pattern $6\sqrt{3}\times 6\sqrt{3}R30°$ formed by the overlapping silicon and carbon atoms. (b) Final configuration: geometrical pattern of Si-C bonds established at the graphene nanoflake-substrate interface. The bonds formed by the initially overlapping atoms are marked by cyan color and the bonds formed by the atoms which do not overlap in the initial configuration are marked by red color. The rotation angle is $\theta=30°$ and the radius of the graphene nanoflake is $R=84$ Å.

initial configuration. If the overlapping atoms form a lattice, then this lattice serves as a reference for the formation of the covalent bonds between the atoms of the graphene nanoflake and the Si atoms on the substrate.

However, after energy minimization, in addition to the anticipated covalent Si-C bonds formed between the overlapping atoms, we find extra bonds established between the pairs of atoms, which do not belong to the overlapping atoms in the initial configuration. For the rotation angle $\theta=30°$, the initial plane lattice $6\sqrt{3}\times 6\sqrt{3}R30°$ is noticeably altered by the extra bonds [marked in Fig. 8(b) by red color] formed close to the center and at the edge of the graphene nanoflake. In contrast to the $\theta=30°$ case, the triangular lattice pattern $p(4\times 4)$ remains intact, since additional bonds emerge only at the edge of the graphene nanoflake. This triangular lattice represents a domain with a perfect epitaxy [see Fig. 7(b)].

While a perfect triangular lattice is obtained, the natural question arises: whether the size of the perfect epitaxy domain scales proportionally to the radius of the graphene nanoflake. To answer this question, we increase the nanoflake radius (see Fig. 9). We find that the size of the perfect epitaxy domain (~70 Å) is limited by lattice mismatch between the two overlapping hexagonal lattices of the nanoflake and the substrate. The lattice mismatch is estimated as following: in Fig. 10 two overlapping pairs of atoms of the graphene nanoflake and the substrate, AA′ and B′B′ pairs, are shown. The in-plane (lateral) coordinates of the atoms A and A′ coincide by construction, but there is a nonzero, albeit, small in-plane distance between B and B′ atoms, due to lattice mismatch. The distance between the

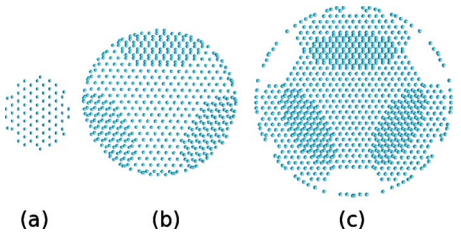

FIG. 9. (Color online) Bond pattern as a function of graphene nanoflake radius, R: (a) $R=56$ Å, (b) $R=124$ Å, and (c) $R=184$ Å. The rotation angle is $\theta=0°$.

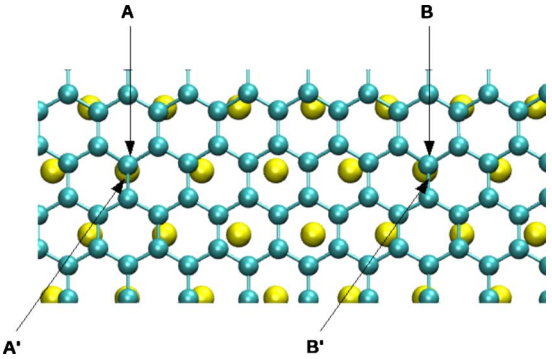

FIG. 10. (Color online) Covalent bonds formed between the overlapping atoms of the nanoflake and substrate. The in-plane (lateral) coordinates of the carbon atom A and silicon atom A′ (B and B′ atoms) overlap. A covalent bond is formed between the pair of AA′ (and BB′) atoms. Graphene nanoflake is rotated by $\theta=0°$.

carbon atoms AB of the graphene hexagonal lattice is given by

$$|AB| = 10a_{\text{C-C}}\cos(\pi/6) = 12.299 \text{ Å}, \quad (4)$$

where $a_{\text{C-C}}=1.4202$ Å is carbon-carbon bond length in graphene lattice. The distance between the silicon atoms A′B′ of the substrate lattice is given by

$$|A'B'| = 4a_{\text{Si-Si}} = 12.323 \text{ Å}, \quad (5)$$

where $a_{\text{Si-Si}}=3.0807$ Å is the silicon-silicon bond length of the top substrate layer. Given the interatomic distances, the lattice mismatch strain is calculated to be

$$\epsilon = \frac{|A'B'|}{|AB|} - 1 = 0.002 \quad (6)$$

and it is 0.2%.

In the absence of lattice mismatch, the Si-C covalent bonds established at the nanoflake-substrate interface form a perfect epitaxy domain. The size of the epitaxy domain is only limited by the diameter of the nanoflake. For brevity sake, the atoms forming bonds of the perfect epitaxy domain at the nanoflake-substrate interface are called the common lattice atoms. In the ideal case with no lattice mismatch, lateral (in-plane) coordinates of the common lattice atoms forming Si-C bonds overlap precisely. But, due to lattice mismatch, the lateral distance between the common atoms increases gradually as one moves away from the center of the graphene nanoflake. At some range one reaches the point where the distance between a pair of carbon and silicon atoms of the common lattice becomes larger than the distance between a pair of carbon and silicon atoms which are not common lattice atoms. In that case the covalent bond formed between these noncommon lattice atoms disrupt the triangular lattice structure of the perfect epitaxy domain. Hence, the perfect epitaxy domain is encircled by a region with rather complex geometrical pattern, which for our purposes is called defected region.

The average lateral distance between the carbon and silicon atoms forming bonds at the boundary of the perfect epitaxy domain is $\Delta=0.15$ Å. This distance sets the limit to the

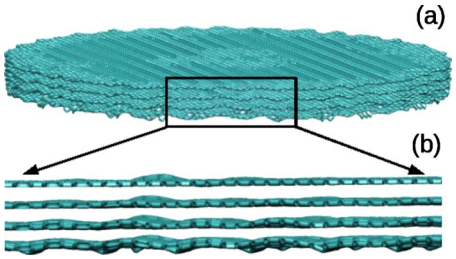

FIG. 11. (Color online) Stack of graphene nanoflakes accommodated on the Si-terminated SiC(0001) substrate. (a) Four graphene nanoflakes. Rotation angle is $\theta=0°$ and the radius of each graphene nanoflake is $R=84$ Å. (b) Morphology of graphene nanoflakes: zoom in for the selected region.

size of the perfect epitaxy domain. By using Δ and the calculated value of lattice mismatch, $\epsilon \simeq 0.002$, one can estimate the radius of the perfect epitaxy domain, L, from

$$L\epsilon = \Delta. \tag{7}$$

We find that the radius of perfect epitaxy domain is about $L \simeq 75$ Å, which is in a good agreement with the radius $L \simeq 70$ Å obtained directly in our simulations.

When we further increase the nanoflake radius, the perfect epitaxy domains reappear again due to periodicity of the hexagonal lattices of the substrate and nanoflake [see Fig. 9(c), which shows the incomplete domains of the perfect epitaxy located at the nanoflake edge]. Those surrounding perfect epitaxy domains have the similar shape and size as the central domain, and, in their turn, are surrounded by the defected regions.

Finally, we put a few nanoflakes on the top of the graphene nanoflake supported by the Si-terminated SiC(0001) substrate (see Fig. 11). The first graphene nanoflake forms covalent bonds with the underlying substrate and can be considered as a buffer layer. The additional graphene nanoflakes do not form bonds with the buffer layer or between themselves. These graphene layers change their initial flat shape to conform to the shape of the buffer layer. This change in the morphology is due to the substantial out-of-plane flexibility of graphene.

IV. CONCLUSIONS

We have studied the epitaxial relation of a graphene nanoflake accommodated on the Si-terminated 4H-SiC(0001) substrate using a semiempirical many-body Tersoff potential. We have found that the covalent bonds form intricate two-dimensional patterns at the interface between the nanoflake and substrate. Among the diverse bond patterns obtained by rotation of the graphene nanoflake, we identify one with a perfect triangular lattice. The size of perfect epitaxy domain is about 70 Å, which is set by the lattice mismatch between the common hexagonal lattice of the nanoflake and the substrate. The bond pattern formed at the interface between the substrate and graphene nanoflake with large radius contains regularly distributed domains with perfect epitaxy surrounded by defected regions.

ACKNOWLEDGMENTS

This work was funded by the Agency for Science, Research and Technology (A*STAR), Singapore. Graphic images were made with the visual molecular dynamics (VMD) visualization package (Ref. 44). The large-scale atomic/molecular massively parallel simulator (LAMMPS) (Ref. 37) code used in our simulations was distributed by Sandia National Laboratories.

*sorkinv@ihpc.a-star.edu.sg

[1] K. S. Novoselov, A. K. Geim, S. V. Morozov, D. Jiang, Y. Zhang, S. V. Dubonos, I. V. Grigorieva, and A. A. Firsov, Science **306**, 666 (2004).
[2] J. C. Meyer, A. K. Geim, M. I. Katsnelson, K. S. Novoselov, T. J. Booth, and S. Roth, Nature (London) **446**, 60 (2007).
[3] A. H. Castro Neto, F. Guinea, N. M. Peres, K. S. Novoselov, and A. K. Geim, Rev. Mod. Phys. **81**, 109 (2009).
[4] A. K. Geim, Science **324**, 1530 (2009).
[5] C. Berger *et al.*, J. Phys. Chem. B **108**, 19912 (2004).
[6] A. K. Geim and K. S. Novoselov, Nature Mater. **6**, 183 (2007).
[7] J. Moon, D. Curtis, D. W. M. Hu, C. McGuire, P. Campbell, G. Jernigan, J. Tedesco, B. VanMil, R. Myers-Ward, and C. Eddy, IEEE Electron Device Lett. **30**, 650 (2009).
[8] P. Sutter, Nature Mater. **8**, 171 (2009).
[9] M. Zarenia, J. M. Pereira, A. Chaves, F. M. Peeters, and G. A. Farias, Phys. Rev. B **81**, 045431 (2010).
[10] D. A. Bahamon, A. L. C. Pereira, and P. A. Schulz, Phys. Rev. B **79**, 125414 (2009).
[11] M. Manninen, H. P. Heiskanen, and J. Akola, Eur. Phys. J. D **52**, 143 (2009).
[12] H. P. Heiskanen, M. Manninen, and J. Akola, New J. Phys. **10**, 103015 (2008).
[13] Z. Jiang, Y. Zhang, H. L. Stormer, and P. Kim, Phys. Rev. Lett. **99**, 106802 (2007).
[14] A. Matulis and F. M. Peeters, Phys. Rev. B **77**, 115423 (2008).
[15] W. L. Wang, S. Meng, and E. Kaxiras, Nano Lett. **8**, 241 (2008).
[16] O. Hod, V. Barone, and G. E. Scuseria, Phys. Rev. B **77**, 035411 (2008).
[17] B. Trauzettel, D. V. Bulaev, D. Loss, and G. Burkard, Nat. Phys. **3**, 192 (2007).
[18] L. A. Ponomarenko, F. Schedin, M. I. Katsnelson, R. Yang, E. W. Hill, K. S. Novoselov, and A. K. Geim, Science **320**, 356 (2008).
[19] P. G. Silvestrov and K. B. Efetov, Phys. Rev. Lett. **98**, 016802 (2007).
[20] F. Muñoz-Rojas, D. Jacob, J. Fernández-Rossier, and J. J. Palacios, Phys. Rev. B **74**, 195417 (2006).
[21] J. Wurm, A. Rycerz, I. Adagideli, M. Wimmer, K. Richter, and H. U. Baranger, Phys. Rev. Lett. **102**, 056806 (2009).
[22] J. Güttinger, C. Stampfer, F. Libisch, T. Frey, J. Burgdörfer, T. Ihn, and K. Ensslin, Phys. Rev. Lett. **103**, 046810 (2009).
[23] F. Libisch, C. Stampfer, and J. Burgdorfer, Phys. Rev. B **79**, 115423 (2009).

[24] J. H. Bardarson, M. Titov, and P. W. Brouwer, Phys. Rev. Lett. **102**, 226803 (2009).
[25] M. Ishigami, J. H. Chen, W. G. Cullen, M. S. Fuhrer, and E. D. Williams, Nano Lett. **7**, 1643 (2007).
[26] D. Usachov, A. M. Dobrotvorskii, A. Varykhalov, O. Rader, W. Gudat, A. M. Shikin, and V. K. Adamchuk, Phys. Rev. B **78**, 085403 (2008).
[27] U. Stöberl, U. Wurstbauer, W. Wegscheider, D. Weiss, and J. Eroms, Appl. Phys. Lett. **93**, 051906 (2008).
[28] F. Varchon, P. Mallet, J.-Y. Veuillen, and L. Magaud, Phys. Rev. B **77**, 235412 (2008).
[29] V. Sorkin and Y. W. Zhang, Phys. Rev. B **81**, 085435 (2010).
[30] D. Hull and D. J. Bacon, *Introduction to Dislocations* (Butterworth-Heinemann, London, 2002).
[31] J. Tersoff, Phys. Rev. B **39**, 5566 (1989).
[32] J. Zang, A. Treibergs, Y. Han, and F. Liu, Phys. Rev. Lett. **92**, 105501 (2004).
[33] M. J. Lopez, I. Cabria, N. H. March, and J. A. Alonso, Carbon **43**, 1371 (2005).
[34] E. B. Halac, M. Reinoso, A. G. Dall'Asen, and E. Burgos, Phys. Rev. B **71**, 115431 (2005).
[35] J. W. Kang, J. J. Seo, and H. J. Hwang, J. Nanosci. Nanotechnol. **2**, 687 (2002).
[36] V. I. Ivashchenko, P. E. A. Turchi, V. I. Shevchenko, and O. A. Shramko, Phys. Rev. B **70**, 115201 (2004).
[37] S. J. Plimpton, J. Comput. Phys. **117**, 1 (1995).
[38] P. Mélinon, B. Masenelli, F. Tournus, and A. Perez, Nature Mater. **6**, 479 (2007).
[39] Q. Lu and R. Huang, Phys. Rev. B **81**, 155410 (2010).
[40] C. K. Gan and D. J. Srolovitz, Phys. Rev. B **81**, 125445 (2010).
[41] R. C. Thompson-Flagg, M. J. B. Moura, and M. Marder, EPL **85**, 46002 (2009).
[42] K. V. Bets and B. I. Yakobson, Nano Res. **2**, 161 (2009).
[43] V. B. Shenoy, C. D. Reddy, A. Ramasubramaniam, and Y. W. Zhang, Phys. Rev. Lett. **101**, 245501 (2008).
[44] W. Humphrey, A. Dalke, and K. Schulten, J. Mol. Graphics **14**, 33 (1996).